Yang, L.; Hort, N.; Laipple, D.; Hoeche, D.; Huang, Y.; Kainer, K.U.; Willumeit, R.; Feyerabend, F.:

Element distribution in the corrosion layer and cytotoxicity of alloy Mg–10Dy during in vitro biodegradation

In: Acta Biomaterialia (2013) Elsevier

DOI: 10.1016/j.actbio.2012.10.001

Element distribution in corrosion layer and cytotoxicity of Mg-10Dy alloy during *in vitro* bio-degradation

Lei Yang *, Norbert Hort, Daniel Laipple, Daniel Höche, Yuanding Huang, Karl Ulrich Kainer, Regine Willumeit, Frank Feyerabend

Helmholtz Zentrum Geesthacht, Institute of Materials Research, Max-Planck-Str. 1, D-21502 Geesthacht, Germany

Abstract

The present work investigates the corrosion behaviour, the element distribution in corrosion layer and the cytocompatibility of Mg-10Dy alloy. The corrosion experiments were performed in a cell culture medium (CCM) under cell culture conditions, which is close to *in vivo* environment. The element distribution on the surface as well as on the cross section of the corrosion layer was investigated using SEM, EDX, XPS and XRD. The cytocompatibility of Mg-10Dy alloy with primary human osteoblasts was evaluated by MTT, cell adhesion and live/dead staining tests. The results show Dy enriches in the corrosion layer and the P and Ca content gradually reduce from the surface to the bottom of the corrosion layer. In addition, it is found that large amount of $MgCO_3 \cdot 3H_2O$ are formed in the corrosion layer after 28 days of immersion. Both the extracts and Dy-enriched corrosion layer of Mg-10Dy alloy show no cytotoxicity to primary human osteoblasts.

Keywords: Mg-10Dy alloy, in-vitro corrosion, element distribution, cytocompatibility

* Corresponding author Address:

Helmholtz Zentrum Geesthacht, Magnesium Innovation Centre, Institute of Materials Research, Max-Planck-Str. 1, D-21502 Geesthacht, Germany; E-mail address: lyang0522@gmail.com

1 Introduction

A number of recent studies emphasise the possibilities of using Mg alloys as a new class of degradable biomaterials for orthopaedic applications [1-4]. As Mg-RE (RE=rare earth) alloys have shown a good combination of mechanical and corrosion properties, extensive investigations have been performed on RE-containing Mg alloys, such as WE43 [5, 6] (4wt% yttrium, 3wt% RE), LAE442 (4wt% lithium, 4 wt% aluminum, 2wt% RE) [7, 8], Mg-Gd [9], Mg-Dy [10, 11], Mg-Y-Zn [12, 13] and Mg-Nd-

Zn-Zr alloys[14, 15], for medical applications. Moreover, WE43 alloy has already been used in clinical studies [16].

It is essential to investigate corrosion layers, especially the distribution of alloying elements in the layer and their influence on the biocompatibility of Mg-RE alloys used in biomedical applications. The corrosion layer acts as the interface between Mg alloys and body fluids as well as body tissues. It plays a very important role in determining both the corrosion behavior and the biocompatibility of Mg alloys. Investigations have already been conducted on the corrosion layers of Mg alloys, such as Mg-Mn-Zn [17], AZ31 [18] and WE43 [19]. These investigations focus on the microstructure and composition of the surface of the corrosion layer. In order to further understand the biodegradation process and the distribution of different elements across the corrosion layer, it is also necessary to investigate the cross section of the corrosion layer. Previous investigation on the cross sections of corrosion layer of pure Mg samples has shown that the distributions of the elements are heterogeneous [20].

Dy is one of the best tolerated RE elements based on *in vitro* study [21] and has very high solubility in Mg (maximum 25.3 wt.%) [22]. The previous work on Mg-Dy alloys shows that solution heat treated Mg-10Dy alloy has a good combination of mechanical and corrosion properties [10]. Hence, solution heat treated Mg-10Dy alloy, in which all the second phase are dissolved into the Mg matrix, is selected in the present work for further investigation. The composition and element distribution on the surface and on the cross section of the corrosion layer were investigated. Furthermore, the cytocompatibility of extracts and corrosion layer was evaluated. As one of the potential applications of Mg-10dy alloy is as bone fixtures, osteoblasts were used in the cytocompatibility tests.

2 Experimental procedures

2.1 Materials preparation

High-purity Mg (MEL, UK, 99.94%) was molten in a mild steel crucible under a protective gas atmosphere (Ar + 2% SF_6). 10 wt.% (1.6 at.%) of pure Dy (Grirem, Beijing, China, 99.5%) was added at a melt temperature of 720 ^{o}C . The melt was then mechanically stirred with a stirrer rotating at 200 rpm for 30 min. Permanent mould direct chill casting technique [23] was used to prepare the ingot (20 cm×12

cm× 6 cm). Pure Mg was prepared using the same melting process as a reference material for corrosion rate and cytocompatibility tests. Solution treatment was performed on Mg-10Dy alloy at 520 °C for 24 hours. The chemical composition of pure Mg and Mg-10Dy alloy was analyzed using X-ray fluorescence (XRF) analyzer (Bruker AXS S4 Explorer, Germany) and spark optical emission spectroscopy (Spectrolab M9 Kleve, Germany) and is listed in Table 1

2.2 Corrosion tests

The specimens for corrosion tests were prepared by grinding each side of the sample with 2400 grit emery paper, and then degreased with ethanol and dried in air. Three samples were used for each corrosion conditions.

The corrosion experiments were conducted under sterile conditions. The samples were sterilized in a solution of 70% ethanol for 15 min. After drying, each sample was immersed in a cell culture medium (CCM) consisting of Dulbecco's modified eagle medium (DMEM) Glutamax-I (Life Technologies, Darmstadt, Germany) and 10% fetal bovine serum (FBS, PAA Laboratories, Linz, Austria). The samples were then incubated in an incubator (Heraeus BBD 6620, Thermo Fisher Scientific, Schwerte, Germany) under cell culture conditions (37°C, 21% O_2, 5% CO_2, 95% rH). The ratio of corrosion medium to surface area of samples was 1.5 mL/cm^2. The composition of DMEM is shown in Table 2. After immersion for up to 28 days without changing the medium, the samples were cleaned with distilled water, dried and kept in a vacuum drying chamber. In weight loss measurement, the corrosion products of specimens after immersion for 3, 7 and 14 days were removed by immersing the corroded specimens in a chromic acid solution (180 g/l) for 20 min at room temperature. Corrosion rate was calculated in millimeter per year (mm/y) with the following equation:

$$CR = \frac{8.76 \times 10^4 \times \Delta \mathrm{g}}{\mathrm{A} \cdot t \cdot \rho} \quad (1)$$

where Δg is weight change in g, A is surface area in cm^2, t is immersion time in hours (h) and ρ is density of the alloy in g·cm^{-3}.

2.3 Characterization of corrosion layer

The macro corrosion morphology was examined using optical microscopy. The observation of micro-corrosion morphology and the analysis of corrosion layer

composition were performed using a Zeiss Ultra 55 (Carl Zeiss GmbH, Oberkochen, Germany) scanning electron microscope (SEM) equipped with energy dispersive X-ray analysis (EDX) at an operating voltage of 15 KV. The thickness of the corrosion layer was measured using a coating thickness gauge (MiniTest 600, ElectroPhysik, Germany).

The cross section of the corroded sample (after 3 days immersion) was prepared by cutting the sample with 30 keV gallium focused ion beam (FIB), equipped on a SEM (Auriga, Zeiss, Oberkochen, Germany). To prevent damage to the corrosion layer and obtain precise cutting along the corrosion layer, a layer of platinum was deposited on the surface of corrosion layer. The morphology observation, line scanning and mapping of the cross section of the corrosion layer were performed directly after cutting, operating at 15 KV.

X-ray induced photoelectron spectroscopy (XPS) measurements were carried out on a Kratos Axis Ultra DLD (Kratos Analytical Ltd., Manchester, UK) attached with a 15 KV X-ray gun using monochromatic Al Kα radiation. The samples of Mg-10Dy alloy and pure Dy metal immersed in the CCM under cell culture conditions for 24 h were used for XPS studies. Samples were cleaned with distilled water and dried in vacuum. The XPS measurements were conducted on an area of 700 μm × 300 μm with pass energy of 40 eV at the regions of measurements and 160 eV for survey scans. As a result of the nonconductive nature of the corrosion products, a charge neutralizer was used to correct the chemical shifts caused by charging. Argon ions (4000 eV), with an etching rate of about 40nm/min, were used to etch the specimens in order to investigate the composition of corrosion layer at different depth. Curve fitting of the spectra was conducted with Casa 2.3.15 software (Casa Software Ltd., Teighnmouth, Devon, UK, 2003). Element binding energy database used is the NIST Standard Reference Database 20, Version 3.5

X-ray diffraction (XRD) was used to identify the phases in the corrosion layer. The XRD measurements were carried out using a diffractometer (Siemens D5000, Germany) with Cu K-α_1 radiation (wavelength k = 0.15406 nm). The operating voltage and current were 40 kV and 40 mA, respectively. The step size was 0.02 degree with a dwell time of 3 s.

2.4 Isolation and culture of cells

2.4.1 SaoS-2 cells

To save time of isolation and culture of primary human osteoblasts, human osteosarcoma cell line SaoS-2 (human osteoblast-like cells) was used to evaluate the cytotoxicity of Dy^{3+} ions. The human osteosarcoma cell line SaoS-2 was obtained from the European collection of cell cultures (ECACC, Salisbury, UK). The cells were cultured under standard cell culture conditions in McCoy's 5A medium (Life Technologies, Darmstadt, Germany) with 15% FBS. Cells were passaged at subconfluency (70 – 80%) and reseeded in a density of 2 x 10^4 cells/cm^2. For cell culture experiments cells after the 5^{th} passage were used.

2.4.2 Primary human osteoblasts

Osteoblasts were grown out of bone chips from a patient undergoing total hip arthroplasty following the protocol of Gallagher [24]. The isolation protocol was approved by the local ethic committee. In brief, cancellous bone was removed from the femoral head with bone rongeurs in pieces of about 5 mm diameter. Bone marrow and non-bone components are removed by thoroughly vortexing in phosphate buffered solution (PBS) repeatedly for 30 s, with continuous replacement of the PBS. After the bone fragments were white, ivory-like in appearance they were cultured in DMEM Glutamax-I with 10% FBS,1% penicillin, and 100 mg/L streptomycin (Life Technologies, Darmstadt, Germany) for about 10 days without changing the medium. Thereafter medium was changed every 2–3 days. Passage was done at 70–80% confluence. Experiments were performed with cells in the 2nd passage.

2.5 Evaluation of cytocompatibility

2.5.1 Specimen preparation

Cylindrical specimens with a diameter of 10 mm and a height of 1.5 mm were prepared by electrical discharge machining. Both sides of these specimens were ground with 2400 grit emery paper and ultrasonically cleaned in 100% ethanol and dried in air. Before the tests, all specimens were sterilized in 70% ethanol for 15 min.

2.5.2 Cytocompatibility of $DyCl_3$ and extracts

To evaluate possible cytotoxic effect of Dy^{3+}, a cytotoxicity assay was performed. $DyCl_3$ (Sigma-Aldrich-Chemie, Taufkirchen, Germany) was dissolved in distilled water

at a concentration of 1 M and sterile filtered. By dilution the final concentrations from 10 µM to 7 mM were obtained. SaoS-2 cells were seeded in 96-well plates (Nunc, Wiesbaden, Germany) in a density of 2 x 10^3 per well/100 µL and incubated at 37°C for 24 hours to allow cell adhesion. Thereafter, concentrations in the given range of $DyCl_3$-solution were added to the wells. After another 48 hours of incubation time, cell viability was measured by MTT (methylthiazolyldiphenyl-tetrazolium bromide, Life Technologies, Darmstadt, Germany). 10 µL of the MTT-solution (5 mg/mL MTT in phosphate buffered saline (PBS)) was added and incubated for 5 hours. Then 1 mL of 10% SDS in 0.01M HCl (Merck, Darmstadt, Germany) was added, followed by incubation overnight in a humidified atmosphere (37° C, 5% CO_2). The solubilized formazan product was photometrically quantified using an ELISA reader (Tecan Sunrise, TECAN Deutschland GmbH, Crailsheim, Germany) at the absorption wavelength 570 nm with a reference wavelength of 655 nm. The same experiments were performed without cells to exclude an influence of the salt concentrations on the MTT-assay. For each concentration 16 replicates were performed.

To evaluate the cytocompatibility of the dissolved corrosion products of Mg-10Dy alloy, cell viability in extracts was measured with MTT tests. Extracts were prepared by immersing specimens into CCM (1.5 ml/cm^2) for 72 h under cell culture conditions. Then the extracts were centrifuged and the supernatant fluid was used as the tested extracts. Osteoblasts were seeded in 96-well plates (Nunc, Wiesbaden, Germany) in a density of 2,500 per well/100 µl and incubated at 37 °C for 24 h to allow cell adhesion. Then the medium was replaced by extracts with concentration of 25%, 50%, 75% and 100%. The CCM was used as the control group, and the extracts without cells were used as the background control. After 2 and 6 days incubation time, cell viability was measured by the MTT test as described before. For each concentration 4 replicates were used. Before MTT test, the tested extracts were replaced with fresh CCM to avoid interaction between extracts and MTT solution [25].

2.5.3 Cytocompatibility of the corrosion layer

To evaluate the cytocompatibility of the corrosion layer of the Mg-10Dy alloy, cell adhesion and live/dead staining tests were performed. Pure Mg specimens were investigated as a reference. Prior to cell seeding, specimens were pre-incubated for 2 h (cell adhesion test) and 3 days (live/dead staining) in CCM under cell culture condition. Agarose coating was prepared on 12-well-plates (Nunc, Wiesbaden,

Germany) to avoid growth of cells on the plates. Osteoblasts were seeded on top of the specimens in the 12-well-plates in 50 µl solution at a density of 100,000 cells per specimen and incubated for 40 min for the cells to settle down. And then, 3 ml CCM was added to each well and the CCM was refreshed every 3 days.

Cell adhesion

After 3 and 7 days incubation, the specimens were washed with PBS and then immersed in 2.5% glutaraldehyde solution over night to fix the cells. The specimens were then immersed into 1% osmium tetroxide for 30 min for staining. Gradual dehydration was carried out in a graded aqueous alcohol series from 20 to 100 vol.% isopropanol (2-propanol, Merck; Darmstadt, Germany). Finally, the specimens were dried via critical point drying in isopropanol (Leica EM CPD030, Leica Mikrosysteme, Wetzlar, Germany). Morphology of cells on the specimens was observed using the SEM operated at 1 KV. For each condition 2 replicates were used.

Live/dead staining

LIVE/DEAD Viability/Cytotoxicity Kit (Life Technologies, Darmstadt, Germany) for mammalian cells was used for staining. The staining solution consisted of 98.6 vol.% CCM, 0.4 vol.% Calcein AM and 1 vol.% Ethidiumhomodimer-1. After incubation for 3 and 7 days, the specimens were washed with PBS and then covered with the the staining solution. The samples were then incubated in cell culture conditions for 20 min, after which the staining solution was replaced with the CCM. For each condition 2 replicates were used. Fluorescence microscopy (TI Eclipse, Nikon, Düsseldorf, Germany) was used to record the fluorescence images. 4 images were taken randomly and used for cell viability calculation using the following equation:

$$CV = \frac{NL}{NL + ND} \times 100\% \qquad (2)$$

where CV is the cells viability, NL is the number of live cells and ND is the number of dead cells.

3 Results

3.1 Corrosion morphology

The corrosion morphology of Mg-10Dy alloy after immersion for different time periods is shown in Fig. 1. Large number of cracks had formed on the surface of all samples due to dehydration during drying. After immersion for 1 day, the surface of the sample was fully covered by a corrosion layer. Some initial pitting corrosion was

observed at places covered by locally piled corrosion products as indicated by arrows in (Fig. 1 (a)). The pitting corrosion was inhibited by the corrosion layer and did not develop into the regions of localized corrosion with further immersion (Fig. 1 (b)). After immersion for 14 days, the morphology of the corrosion layer remained uniform (Fig. 1 (c)) and no localized corrosion was observed on the surface of Mg-10Dy alloy after removing corrosion products (Fig. 1 (d)).

3.2 Thickness and composition of corrosion layer

Fig. 2 (a) shows the thickness of the corrosion layer on the surface of Mg-10Dy alloy and pure Mg as a function of immersion time. The growth of corrosion layer thickness shows similar trend for pure Mg and Mg-10Dy alloy. The thickness of corrosion layer increases rapidly to about 9 μm after immersion for 3 days. Thereafter, the growth rate becomes slower and remains linear until 11 days. After immersion for 11 days the thickness of the corrosion layer increases rapidly again, and reaches about 75 μm after immersion for 28 days for Mg-10Dy alloy. The corrosion rate of both pure Mg and Mg-10Dy alloy reduces with increased immersion time (Fig. 2 (b)). However, the corrosion rate of Mg-10Dy alloy decreases faster than that of pure Mg. After immersion for 3 days, the corrosion rates of both pure Mg and Mg-10Dy alloy are about 1 mm/year. After immersion for 14 days, the corrosion rates reduce to 0.75 and 0.56 mm/year, respectively for pure Mg and Mg10Dy.

The distribution of the various elements in the surface of the corrosion layer of Mg-10Dy is shown in Fig. 3. After immersion for 1 day, majority of the signal collected by EDX is from the Mg substrate as the corrosion layer is very thin (about 2 μm as shown in Fig. 2 (a)). As a result, the composition of the corrosion layer analyzed by EDX contains around 60 at.% Mg and only small amounts of other elements such as P and Ca. When the immersion time is between 3 and 11 days, the contents of all the elements (Mg, Dy, O, C, P and Ca) remain at the same level on the surface of corrosion layer although the thickness of corrosion layer increases. The Dy is enriched on the surface of the corrosion layer with around 12 at.%, which is about 7 times higher than that contained in the alloy substrate (1.6 at.%). Once the immersion time exceeds 14 days, the contents of P, Ca and Dy reduces while the content of C and O increases in the corrosion layer.

3.3 Cross section morphology and element distribution in the corrosion layer

After immersion for 3 days, the surface and cross-section of the corrosion layer are shown in Fig. 4. The surface with the platinum deposition is shown in Fig. 4a, and the cutting was made at the platinum deposition. The cross section of the cut sample shown in Fig. 4b clearly show the various features such as platinum deposition, corrosion layer, interface and the substrate. The measured thickness of the corrosion layer was about 7.5 μm, which is consistent with results in Fig. 2 (a). Some cavities are also observed at the interface between the corrosion layer and substrate (Fig. 4 (c)).

The EDX map showing the distribution of elements in the corrosion layer is shown in Fig. 5. N and C distribute mainly on the surface of corrosion layer. The amount of P and Ca at the surface of the corrosion layer is higher than that near the bottom of the corrosion layer. Mg and Dy distribute homogeneously in the corrosion layer. The intensity of Dy in the corrosion layer is much higher than that in the Mg-10Dy substrate. In order to further understand the trend of element distribution in the corrosion layer, EDX line scanning was conducted (Fig. 6). The line scanning starts from A and ends at B for the corrosion layer as indicated. The line segment before A is the platinum layer deposited on the samples and the segment after B is Mg-10Dy alloy substrate. The C and N contents are very high on the surface of corrosion layer and reduce dramatically inside the corrosion layer. The O content is higher at the interface between the corrosion layer and Mg-10Dy substrate. This indicates the possibility of oxygen driven corrosion process occurred. Both P and Ca content reduce gradually from the surface to the bottom of corrosion

3.4 XPS investigation

The XPS results are presented in the form of elemental depth profiles recorded for sputtering times of 0-5000s (Fig. 7). After 5000s sputtering the XPS peaks detected changes both in intensity and types, suggesting that the alloy substrate was reached. The peak detected after 5000s sputtering at the binding energy for the Ca (2p) is from the Mg (auger KLL) rather than from Ca. Peaks of C and N were identified on the surface of corrosion layer and no C and N peaks were detected after sputtering for 1000s. Both Dy and Mg peaks show similar intensities through the corrosion layer. The nature of Dy peak changes after sputtering for 5000s as the alloy substrate is

reached. The peak intensities of the P and Ca reduce from the surface to the bottom of the corrosion layer. The XPS results are consistent with that of EDX line scanning and mapping. The O peak detected changes its shape depending on the sputtering time (Fig. 7 (O 1s)). This is due to overlapping of three different peaks containing O. These peaks can be related to O^{2-}(528.8 eV), OH^- (531.2 eV) and PO_4^{3-} (533.5 eV), respectively.

Since Mg and Dy are present in the Mg-10Dy alloy, it is difficult to identify the chemical state of Dy in the corrosion products. To investigate the chemical state of Dy in the corrosion layer, the XPS analysis was carried out on the surface of pure Dy metal after immersion in the CCM for 1 day (Fig. 8). The O 1s peak is split into two clear broad peaks. Due to the multi split orbits, the peaks shape is a result of collection. At lower binding energy, peak position of the O 1s peak is identified at BE=528.8 eV, corresponding to Dy-O bonding of Dy_2O_3. At higher binding energy, the peak position of the O 1s peak is observed at BE=531.3 eV, corresponding to Dy-OH binding of $Dy(OH)_3$ [26, 27]. The Dy-containing corrosion products on pure Dy are a mixture of Dy_2O_3 and $Dy(OH)_3$. Based on these results, it can also be deduced that the Dy-containing corrosion products in the corrosion layer of the Mg-10Dy alloy likely be a mixture of Dy_2O_3 and $Dy(OH)_3$.

3.5 XRD

Fig. 9 shows the XRD spectra of the corrosion layers of the Mg-10Dy samples after immersion for 14 and 28 days. After immersion for 14 days, only pure Mg is identified in the XRD profile which indicating that the corrosion layer is penetrated by the X-ray (Fig. 9 (a)). As a result, most of the collected signals are from the Mg matrix. However, after 28 days of immersion the intensity of Mg peaks is drastically reduced, and peaks for $MgCO_3 \cdot 3H_2O$ are identified as shown in Fig. 9 (b).

3.6 Cytocompatibility

The viability of SaoS-2 cells in CCM with different concentrations of $DyCl_3$ is shown in Fig. 10. With the increase of $DyCl_3$ concentration up to 4000 µm there is no change in cell viability. However, a further increase of $DyCl_3$ concentration to 5000 µM results in a dramatic decrease in cell viability to around 60%.

The relative cell viability of osteoblasts after incubation in extracts with different concentration for 2 and 6 days is presented in Fig.11. Similar cell viability is observed for 25% and 50% extracts. Further increase in concentration of extracts from 50% to

100% reduces the cell viability from 117% to ~80%. Although the decrease of cell viability is observed, all the concentrations of extracts have no cytotoxicity according to ISO standard (cell viability>75%) [28].

Cell morphology on the surfaces of specimens after culture for 3 days and 7 days are shown in Fig. 12. After culture for 3 days, a large number of cells are observed on the surfaces of both pure Mg and Mg-10Dy (Fig. 12 (a, c)). The cells are well-spread and adhered to the surface on both pure Mg and Mg-10Dy (Fig. 12 (b, d)). After culture for 7 days, no negative effect due to Dy enrichment on cells is observed.

To further examine the influence of the Dy-enriched corrosion layer on the cell viability, live/dead staining method was used. The compositions of the corrosion layer are found stable after immersion for 3 days in CCM, and hence the specimens were pre-incubated in CCM for 3 days prior to the cells seeding. Fig. 13 and Fig. 14 show the live and dead cells on pure Mg and Mg-10Dy alloy after culture for 3 and 7 days, respectively. Live and dead cells were stained green and red, respectively. A large number of live cells and only a few dead cells are observed on both the pure Mg and Mg-10Dy alloy after culture for 3 days (Fig. 13). Even after 7 days of culture, the trend remains same. The quantification of cell viability on pure Mg and Mg-10Dy alloy is listed in Table 3. After 3 days, the cell viability is about 88.2% for cells on pure Mg and 91.6% on Mg-10Dy alloy. After 7 days, the cell viability is around 93% on both pure Mg and Mg-10Dy alloy. These results confirm that the corrosion layer enriched with Dy in Mg-10Dy alloy does not show any cytotoxicity.

4 Discussion

4.1 Corrosion rate and morphology

It is well established that, in the as-cast condition, the corrosion rate of Mg-RE alloys increases with increase in RE amount due to the increased galvanic effect between Mg matrix and Mg-RE precipitates [29, 30]. Solution treatment eliminates or reduces galvanic corrosion due to the dissolution of the Mg-RE precipitates in to Mg matrix [31, 32]. Previous study shows that the $Mg_{24}Dy_5$ precipitates form a galvanic couple with the Mg matrix and cause pitting corrosion [10]. Due to that reason, in the present work, solution heat treated Mg-10Dy alloy was selected to avoid galvanic corrosion. The electrochemical potential of Dy is -2.35 V, which is similar to that of Mg (-2.37 V). This indicates that elemental Dy would not cause micro-galvanic corrosion of the α-

Mg matrix if Dy is in solid solution in α-Mg matrix. Very tiny pitting was observed in the initial stage of corrosion (Fig. 1 a), but it did not develop further. Since there is no second phase in the tested Mg-10Dy alloy, the observed tiny pitting corrosion is not caused by the galvanic effect due to the second phase. This kind of pitting might be caused by the chemical inhomogeneity in the alloy. The corrosion rate of Mg-10Dy (T4) alloy is slightly less than that of pure Mg in CCM under cell culture conditions (Fig. 2 (b)). This could be due to the incorporation of stable Dy_2O_3 and $Dy(OH)_3$ into the corrosion layer. It is reported that Y dissolved in the Mg matrix can increase the protective nature of the surface film especially in a mild solution [12, 33, 34].

The corrosion rate of a series of Mg alloys was investigated in Minimum Essential Medium (MEM) and the lowest corrosion rate was about 0.65 mm/y observed on AZ91 alloy [35]. In this work, the corrosion rate of Mg-10Dy alloy is found to be about 0.56 mm/y, indicating that Mg-10Dy alloy has low corrosion rate. However, it should be stated that extra protein (10% FBS) was added in the DMEM compared with the MEM used in reference [35], and DMEM was buffered by $NaHCO_3$

Some cavities are observed at the interface between the corrosion layer and substrate (Fig. 4 (c)). The cavities are likely to have formed during the dehydration, as they become larger near to the surface cracks caused by dehydration. During drying, the volume of the corrosion layer reduces, but the substrate remains unchanged. The mismatch at the interface is likely to cause the cavities. Additionally, the oxidation during corrosion could also cause stress and lead to the formation of cavities.

4.2 Corrosion layer composition and elements distribution

In Cl^- ion containing aqueous solution, the corrosion of magnesium occurs through following reactions [36]:

$$Mg \rightarrow Mg^{2+} + 2e^- \quad (3)$$

$$2H_2O + 2e^- \rightarrow H_2 + 2OH^- \quad (4)$$

$$Mg^{2+} + 2(OH)^- \rightarrow Mg(OH)_2 \quad (5)$$

Based on the above reactions, $Mg(OH)_2$ forms in the corrosion layer initially and then transforms into more soluble $MgCl_2$ in the presence of aggressive chloride ions through following reaction:

$$Mg(OH)_2 + 2Cl^- \rightarrow MgCl_2 + 2OH^- \quad (6)$$

Therefore, during corrosion a part of $Mg(OH)_2$ is transformed into Mg ions and

released into the corrosion solution. Another part of $Mg(OH)_2$ is still left in the corrosion layer.

Dy metal is quite electropositive, and has a similar standard potential (-2.35V) to Mg (-2.37V). The main corrosion product for Dy is Dy_2O_3 and a small amount of $Dy(OH)_3$ as detected by XPS (Fig. 8). The following reaction may be deduced.

$$2Dy + 3H_2O \rightarrow Dy_2O_3 + 3\ H_2 \quad (7)$$

$$2Dy + 6H_2O \rightarrow 2\ Dy(OH)_3 + 3\ H_2 \quad (8)$$

Dy_2O_3 is insoluble in water. The solubility product constant (Ksp) for $Dy(OH)_3$ is 1.4×10^{-22}, which is much smaller than that of $Mg(OH)_2$ (5.61×10^{-12}). Thus, Dy_2O_3 and $Dy(OH)_3$ are more likely to remain in the corrosion layer than $Mg(OH)_2$ due to the lower solubility. This results in the enrichment of Dy in the corrosion layer (Fig. 5 and Fig. 6).

Previous studies [17, 37] have shown that the following reaction occurs when Mg is exposed to a solution containing Ca^{2+}, $H_2PO_4^-$ and HPO_4^{2-} ions.

$$Mg^{2+} + Ca^{2+} + PO_4^{3-} \rightarrow Ca_xMg_y(PO_4)_z \quad (9)$$

At the beginning of the corrosion process, equation 9 is dynamically balanced. The formation and dissolution of $Ca_xMg_y(PO_4)_z$ precipitates occur at the same rate. As the immersion time increases, the amount of released Mg^{2+} increases, which provides driving force for the formation of $Ca_xMg_y(PO_4)_z$. For Mg-10Dy alloy, a dense and homogeneous corrosion layer containing Dy_2O_3/ $Dy(OH)_3$ forms during corrosion. This corrosion layer could reduce permeability of Ca^{2+} and PO_4^{3-} ions to the interface between corrosion layer and Mg-10Dy substrate. Ca^{2+} and PO_4^{3-} ions are mainly in the corrosion medium and the surface of corrosion layer. As a result, $Ca_xMg_y(PO_4)_z$ precipitates from mainly on the surface of corrosion layer where a high concentration of Mg^{2+} is prevalent and sufficient Ca^{2+} and PO_4^{3-} ions are present. Higher P and Ca content found on the surface of corrosion layer (Fig. 5 and Fig. 6), agrees with the above analysis.

Under the cell culture conditions, the carbon dioxide causes the formation of H_2CO_3 [20]. It reacts with $Mg(OH)_2$ and stabilizes the pH value of corrosion solution, as follows:

$$H_2O + CO_2 \rightarrow H_2CO_3 \quad (10)$$

$$Mg(OH)_2 + H_2CO_3 \rightarrow MgCO_3 + H_2O \quad (11)$$

$Mg(CO)_3$ forms continuously with the corrosion of Mg. The solubility of $MgCO_3$ is about 220 mg/l [20]. In the early stage of corrosion, the most of the $MgCO_3$ dissolves

into the corrosion solution and less or no $MgCO_3$ accumulates in the corrosion layer. Thus, C is found to be only on the surface of the corrosion layer after immersion for 1 day and 3 days (Fig. 5 and Fig. 7), which could be the $MgCO_3$ corrosion products or contamination from air. With the increase of immersion time, more and more $MgCO_3$ forms and the corrosion solution becomes saturated. Then the $MgCO_3$ accumulates in the corrosion layer and the thickness of the corrosion layer grows rapidly (Fig. 2 (a), after 11 days immersion).This is supported by the high content of C and O detected at the surface of corrosion layer when immersion time exceeds 11 days (Fig. 3). This conclusion is further confirmed by XRD experimental result which demonstrates that $MgCO_3$ is the main corrosion products after 28 days immersion (Fig. 9). Similar result is also obtained in a previous study [20], which reports a large amount of $MgCO_3$ forms in the corrosion layer with a thickness of around 80 µm. Furthermore, many studies shown that large amount of C and O is observed in the corrosion layer of Mg-based implants after long term *in vivo* tests in animal bones [38-41]. This could be due to the buffering effect of CO_2 and formation of $MgCO_3$ in the environment with limited body fluid.

4.3 Cytocompatibility

The biocompatibility of corrosion products is one of the key points for successful application of magnesium alloys as implants. Corrosion products end up in two forms: (i) extracts and (ii) corrosion layer. Thus, the cytocompatibility of extracts and the Dy-enriched corrosion layer of Mg-10Dy alloy were evaluated. To evaluate the effects of corrosion layer on cells we choose two different experimental approaches: (1) an adhesion test during the initial stage of corrosion layer formation and (2) a cell viability examination after the formation of a more or less stable corrosion layer. For both approaches a pre-incubation step was performed (2 hours for adhesion and 3 days for viability). This is due to the fact that during an implantation the first contact of the material will be with blood, which will initiate material corrosion. This scenario is simulated by the short pre-incubation of 2 h in CCM before cell seeding. Moreover, also the effect of the Dy enrichment in the corrosion layer on cells should be determined. Therefore, a pre-incubation time of three days was used in the cell viability test. In this case, the main aim was to have a corrosion layer, which was enriched by Dy and to study its effect on human osteoblast viability.

In the extracts test, although no cytotoxic effects on osteoblasts are observed

based on ISO standard [28], the cell viability decreases to around 80% with the concentration of extracts increases to 100%. This could be caused by the high Mg^{2+} and Dy^{3+} concentration in the extracts. The concentration of released Mg^{2+} and Dy^{3+} in 100% extracts is around 37.5 mM/L and 0.62 mM/L by converting the corrosion rate of Mg-10Dy alloy (the Mg and Dy in the corrosion layer are neglected). The tolerance limit of Dy^{3+}concentration (with 80% cell viability) is about 4 mM/L for SaoS-2 cells (Fig. 10) and about 1 mM/L for human osteosarcoma cell line MG63 [21]. Both of these two Dy^{3+} concentrations are higher than that observed in 100% extracts in the present study. Thus the decreased cell viability should not be caused by Dy^{3+}. The tolerance limit of Mg^{2+} concentration (with 80% cell viability) is about 38 mM/L for mouse macrophages (RAW 264.7), 22 mM/L for MG63 and 39 mM/L for human umbilical cord perivascular (HUCPV) cells [21]. These Mg^{2+} concentrations are close to the Mg^{2+} concentrations measured in the tested extracts. Therefore, the reason for the decreased cell viability should be due to the high Mg^{2+} concentration.

The experimental results show that the accumulation of Dy also does not induce cytotoxic effects. Actually the most toxic forms of metals are generally inorganic non-chelated ions, which are available for uptake into organisms [42]. In the corrosion layer, Dy exists as a mixture of Dy_2O_3 and $Dy(OH)_3$, which can not be absorbed by cells even with direct contacts. Dy_2O_3 shows no appreciable toxicity at a concentration of up to 1000 µg/ml in cytotoxicity studies with BEAS-2B (human bronchial epithelial cells) and L929 cells [43]. Dysprosium (165) hydroxide macroaggregates were developed to utilize the advantages of dysprosium 165 in radiation synovectomy of certain forms of arthritis [44, 45]. Additionally, the Dy complexes were used as the contrast medium for magnetic resonance imaging [46]. Therefore, based on the above discussion the effect of a small amount of Dy in Mg alloys should be tolerable.

However, there is a naturally occurring accumulation of rare earth elements in human bones [47], and it was observed that dysprosium can replace calcium in hydroxyapatite [48]. Before applying rare-earth based alloys therefore more insight in their influence on bone structure and metabolism should be investigated.

5 Summary

In the bio-corrosion layer, the distribution of elements is inhomogeneous from the surface to the bottom of the layer. The corrosion layer is enriched with Dy, which

likely exists as a mixture of Dy_2O_3 and $Dy(OH)_3$. The content of Ca and P decreases gradually from the surface to the bottom of the corrosion layer. Due to the buffering effect of CO_2, $MgCO_3 \cdot 3H_2O$ forms during corrosion and it accumulates in the corrosion layer after the corrosion solution is saturated. Both the extracts and the Dy-enriched corrosion layer of Mg-10Dy alloy cause no cytotoxicity on human osteoblasts.

Acknowledgement

The authors thank to Mr. M. Kieke, Dr. C. Mendis and Dr. A. Srinivasan for helpful discussions. Technical assistance from Mr. W. Punessen and Mrs. G. Salamon is appreciated. Financial support from CSC-Helmholtz scholarship is gratefully acknowledged.

References

[1] Staiger MP, Pietak AM, Huadmai J, Dias G. Magnesium and its alloys as orthopedic biomaterials: A review. Biomaterials 2006;27:1728-34.

[2] Zeng RC, Dietzel W, Witte F, Hort N, Blawert C. Progress and challenge for magnesium alloys as biomaterials. Adv. Eng. Mater. 2008;10:B3-B14.

[3] Witte F, Hort N, Vogt C, Cohen S, Kainer KU, Willumeit R, Feyerabend F. Degradable biomaterials based on magnesium corrosion. Curr. Opin. Solid State Mater. Sci. 2008;12:63-72.

[4] Gu X, Zheng YF. A review on magnesium alloys as biodegradable materials Front. Mater. Sci. China 2010;4:111–15.

[5] Witte F, Kaese V, Haferkamp H, Switzer E, Meyer-Lindenberg A, Wirth CJ, Windhagen H. In vivo corrosion of four magnesium alloys and the associated bone response. Biomaterials 2005;26:3557-63.

[6] Witte F, Fischer J, Nellesen J, Crostack HA, Kaese V, Pisch A, Beckmann F, Windhagen H. In vitro and in vivo corrosion measurements of magnesium alloys. Biomaterials 2006;27:1013-18.

[7] Witte F, Fischer J, Nellesen J, Vogt C, Vogt J, Donath T, Beckmann F. In vivo corrosion and corrosion protection of magnesium alloy LAE442. Acta Biomater. 2010;6:1792-99.

[8] Gruhl S, Witte F, Vogt J, Vogt C. Determination of concentration gradients in bone tissue generated by a biologically degradable magnesium implant. J. Anal. At. Spectrom. 2009;24:181-88.

[9] Hort N, Huang Y, Fechner D, Stomer M, Blawert C, Witte F, Vogt C, Drüker H, Willumeit R, Kainer KU, Feyerabend F. Magnesium alloys as implant materials - Principles of property design for Mg-RE alloys. Acta Biomater. 2010;6:1714-25.

[10] Yang L, Huang Y, Peng Q, Feyerabend F, Kainer KU, Willumeit R, Hort N. Mechanical and corrosion properties of binary Mg–Dy alloys for medical applications. Materials Science and Engineering: B 2011;176:1827-34.

[11] Yang L, Huang Y, Feyerabend F, Willumeit R, Kainer KU, Hort N. Influence of ageing treatment on microstructure, mechanical and bio-corrosion properties of Mg-Dy alloys. Journal of the Mechanical Behavior of Biomedical Materials 2012;13:36-44.

[12] Hanzi AC, Gunde P, Schinhammer M, Uggowitzer PJ. On the biodegradation performance of an Mg-Y-RE alloy with various surface conditions in simulated body fluid. Acta Biomater. 2009;5:162-71.

[13] Hanzi AC, Gerber I, Schinhammer M, Loffler JF, Uggowitzer PJ. On the in vitro and in vivo degradation performance and biological response of new biodegradable Mg-Y-Zn alloys. Acta Biomater. 2010;6:1824-33.

[14] Zhang X, Yuan G, Mao L, Niu J, Fu P, Ding W. Effects of extrusion and heat treatment on the mechanical properties and biocorrosion behaviors of a Mg–Nd–Zn–Zr alloy. Journal of the Mechanical Behavior of Biomedical Materials 2012;7:77-86.

[15] Wang YP, Zhu ZJ, He YH, Jiang Y, Zhang J, Niu JL, Mao L, Yuan GY. In vivo degradation behavior and biocompatibility of Mg-Nd-Zn-Zr alloy at early stage. International Journal of Molecular Medicine 2012;29:178-84.

[16] Hermawan H, Dubé D, Mantovani D. Developments in metallic biodegradable stents. Acta Biomater. 2010;6:1693-97.

[17] Yang L, Zhang E. Biocorrosion behavior of magnesium alloy in different simulated fluids for biomedical application. Mater. Sci. Eng. C 2009;29:1691-96.

[18] Song Y, Shan D, Chen R, Zhang F, Han E-H. Biodegradable behaviors of AZ31 magnesium alloy in simulated body fluid. Mater. Sci. Eng. C 2009;29:1039-45.

[19] Rettig R, Virtanen S. Composition of corrosion layers on a magnesium rare-earth alloy in simulated body fluids. J. Biomed. Mater. Res. 2009;88A:359-69.

[20] Willumeit R, Fischer J, Feyerabend F, Hort N, Bismayer U, Heidrich S, Mihailova B. Chemical surface alteration of biodegradable magnesium exposed to corrosion media. Acta Biomater. 2011;7:2704-15.

[21] Feyerabend F, Fischer J, Holtz J, Witte F, Willumeit R, Drückere H, Vogt C, Hort N. Evaluation of short-term effects of rare earth and other elements used in magnesium alloys on primary cells and cell lines. Acta Biomater. 2010;6:1834-42.

[22] Nayeb-Hashemi AA, Clark JB. Phase Diagram of Binary Magnesium Alloys. Metal Park, OH, USA: ASM International, 1988.

[23] Peng Q, Huang Y, Zhou L, Hort N, Kainer KU. Preparation and properties of high purity Mg-Y biomaterials. Biomaterials 2010;31:398-403.

[24] Gallagher JA. Human osteoblast culture. Methods in molecular medicine 2003;80:3-18.

[25] Fischer J, Prosenc MH, Wolff M, Hort N, Willumeit R, Feyerabend F. Interference of magnesium corrosion with tetrazolium-based cytotoxicity assays. Acta Biomater. 2010;6:1813-23.

[26] Han K, Zhang Y, Cheng T, Fang Z, Gao M, Xu Z, Yin X. Self-assembled synthesis and photoluminescence properties of uniform Dy2O3 microspheres and tripod-like structures. Materials Chemistry and Physics 2009;114:430-33.
[27] Bhuiyan NK, Menghini M, Dieker C, Seo JW, Locquet J, Vitchev R, Marchiori C. Epitaxial Dy2O3 Thin Films Grown on Ge(100) Substrates by Molecular Beam Epitaxy. MRS Proceedings, 1252 , 1252-I03-01 doi:10.1557/PROC-1252-I03-01 2010.
[28] ISO 10993-5 (2009), Biological evaluation of medical devices - Part 5: Tests for in vitro cytotoxicity, International Organization for Standardization.
[29] Birbilis N, Easton MA, Sudholz AD, Zhu SM, Gibson MA. On the corrosion of binary magnesium-rare earth alloys. Corros. Sci. 2009;51:683-89.
[30] Sudholz AD, Gusieva K, Chen XB, Muddle BC, Gibson MA, Birbilis N. Electrochemical behaviour and corrosion of Mg-Y alloys. Corros. Sci.;53:2277-82.
[31] Liang S, Guan D, Tan X. The relation between heat treatment and corrosion behavior of Mg-Gd-Y-Zr alloy. Mater. Des. 2011;32:1194-99.
[32] Chang J-W, Guo X-W, Fu P-H, Peng L-M, Ding W-J. Effect of heat treatment on corrosion and electrochemical behaviour of Mg-3Nd-0.2Zn-0.4Zr (wt.%) alloy. Electrochimica Acta 2007;52:3160-67.
[33] Yao HB, Li Y, Wee ATS. Passivity behavior of melt-spun Mg-Y Alloys. Electrochimica Acta 2003;48:4197-204.
[34] Liu M, Schmutz P, Uggowitzer PJ, Song G, Atrens A. The influence of yttrium (Y) on the corrosion of Mg-Y binary alloys. Corros. Sci. 2010;52:3687-701.
[35] Kirkland NT, Lespagnol J, Birbilis N, Staiger MP. A survey of bio-corrosion rates of magnesium alloys. Corros. Sci. 2010;52:287-91.
[36] Song G, Atrens A. Understanding Magnesium Corrosion: a Framework for Improved Alloy Performance. Adv. Eng. Mater. 2003;5:837-58.
[37] Kuwahara H, Al-Abdullat Y, Mazaki N, Tsutsumi S, Aizawa T. Precipitation of magnesium apatite on pure magnesium surface during immersing in Hank's solution. Materials Transactions 2001;42:1317-21.
[38] Gu XN, Xie XH, Li N, Zheng YF, Qin L. In vitro and in vivo studies on a Mg-Sr binary alloy system developed as a new kind of biodegradable metal. Acta Biomater. 2012;8:2360-74.
[39] Krause A, von der Hoh N, Bormann D, Krause C, Bach FW, Windhagen H, Meyer-Lindenberg A. Degradation behaviour and mechanical properties of magnesium implants in rabbit tibiae. J. Mater. Sci. 2010;45:624-32.
[40] Zhang E, Xu L, Yu G, Pan F, Yang K. In vivo evaluation of biodegradable magnesium alloy bone implant in the first 6 months implantation. J. Biomed. Mater. Res. 2009;90A:882-93.
[41] Huehnerschulte TA, Angrisani N, Rittershaus D, Bormann D, Windhagen H, Meyer-Lindenberg A. In Vivo Corrosion of Two Novel Magnesium Alloys ZEK100 and AX30 and Their Mechanical Suitability as Biodegradable Implants. Materials 2011;4:1144-67.
[42] Fuma S, Takeda H, Takaku Y, Hisamatsu S, Kawabata Z. Effects of dysprosium on the species-defined microbial microcosm. Bull. Environ. Contam. Toxicol. 2005;74:263-72.
[43] Das GK, Zhang Y, D'Silva L, Padmanabhan P, Heng BC, Loo JSC, Selvan ST, Bhakoo KK, Tan TTY. Single-Phase Dy2O3:Tb3+ Nanocrystals as Dual-Modal Contrast Agent for High Field Magnetic Resonance and Optical Imaging. Chemistry of Materials 2011;23:2439-46.
[44] McLaren A, Hetherington E, Maddalena D, Snowdon G. Dysprosium (Dy-165) Hydroxide Macroaggregates for Radiation Synovectomy - Animal Studies. European Journal of Nuclear Medicine 1990;16:627-32.
[45] Edmonds J, Smart R, Laurent R, Butler P, Brooks P, Hoschl R, Wiseman J, George S, Lovegrove F, Warwick A. A comparative study of the safety and efficacy of dysprosium-165 hydroxide macro-aggregate and yttrium-90 silicate colloid in radiation synovectomy--a multicentre double blind clinical trial. Australian Dysprosium Trial Group. Brit. J. Rheumatol. 1994;33:947-53.
[46] Bottrill M, Nicholas LK, Long NJ. Lanthanides in magnetic resonance imaging. Chem. Soc. Rev. 2006;35:557-71.
[47] Zaichick S, Zaichick V, Karandashev V, Nosenko S. Accumulation of rare earth elements in human bone within the lifespan. Metallomics 2011;3:186-94.
[48] Getman EI, Loboda SN, Tkachenko TV, Ignatov AV, Zabirko TF. Substitution of calcium with neodymium and dysprosium in hydroxyapatite structure. Functional Materials 2005;12:6-10.

Figure captions:

Fig. 1. Typical corrosion morphology of Mg-10Dy alloy after immersion for: (a) 1day; (b) 3 days; (c) 14 days. (a) (b) and (c) are SEM secondary electron images and (d) is an optical microscopy picture (after removing the corrosion products).

Fig. 2. (a) Thickness of corrosion layer and (b) Corrosion rate after immersion at different time points.

Fig. 3. Amount of various elements on the surface of the corrosion layer as a function of immersion time (analyzed by EDX): (a) P, Ca and C; (b) Mg, Dy and O.

Fig. 4. SEM images showing the surface and cross-section of corrosion layer (cut with FIB) after immersion for 3 days: (a) cutting position on the surface; (b) cross-section, low magnification; (c) cross-section, high magnification.

Fig. 5. Distribution of elements in the corrosion layer of the specimen after immersion for 3 days (EDX mapping).

Fig. 6. Trend of element distribution in the corrosion layer (analyzed by EDX line scanning). The specimen was immersed for 3 days and cross section was cut with FIB. Bright area in the corrosion layer is due to a charge effect.

Fig. 7. XPS analysis of elements distribution in the corrosion layer of Mg-10Dy specimen after immersion for 1 day. 0-5000 s represents the sputtering time with argon ions before measurement.

Fig. 8. XPS analysis of the corrosion layer on pure Dy metal after immersion in CCM for 1 day (after etching for 100 s).

Fig. 9. XRD spectra of the corrosion layer on the surface of Mg-10Dy alloy after immersion for: (a) 14 days and (b) 28 days.

Fig. 10. Concentration-dependent dose response to exposure to $DyCl_3$ of SaoS-2 cells.

Fig. 11. Relative cell viability of osteoblasts after incubation in extracts for 2 and 6 days.

Fig. 12. Morphology of human osteoblasts on the surfaces of the specimens after culture for 3 days and 7 days: (a, b) pure Mg for 3 days; (c, d) Mg-10Dy for 3 days; (e, f) pure Mg for 7 days; (g, h) Mg-10Dy for 7 days. Prior to the cell seeding, the specimens were pre-incubated in CCM for 2 h.

Fig. 13. Live (green) and dead (red) cells on the surfaces of specimens after culture for 3 days: (a, b) pure Mg; (c, d) Mg-10Dy alloy. Prior to the cell seeding, the specimens were pre-incubated in CCM for 3 days. The images of the live and dead cells were taken from the same locations. The round green circles shown in (a) and (c) are due to hydrogen bubbles.

Fig. 14. Live (green) and dead (red) cells on the surfaces of specimens after culture for 7 days: (a, b) pure Mg; (c, d) Mg-10Dy alloy. Prior to the test, the specimens were pre-incubated in CCM for 3 days. The images of the live and dead cells were taken from the same location.

Table captions:

Table 1 Detailed composition and impurity levels of Mg-10Dy alloy and pure Mg used in this work (wt.%).

Table 2: Composition of DMEM (mg/L).

Table 3: Quantification of cell viability on the surfaces of pure Mg and Mg-10Dy alloys.

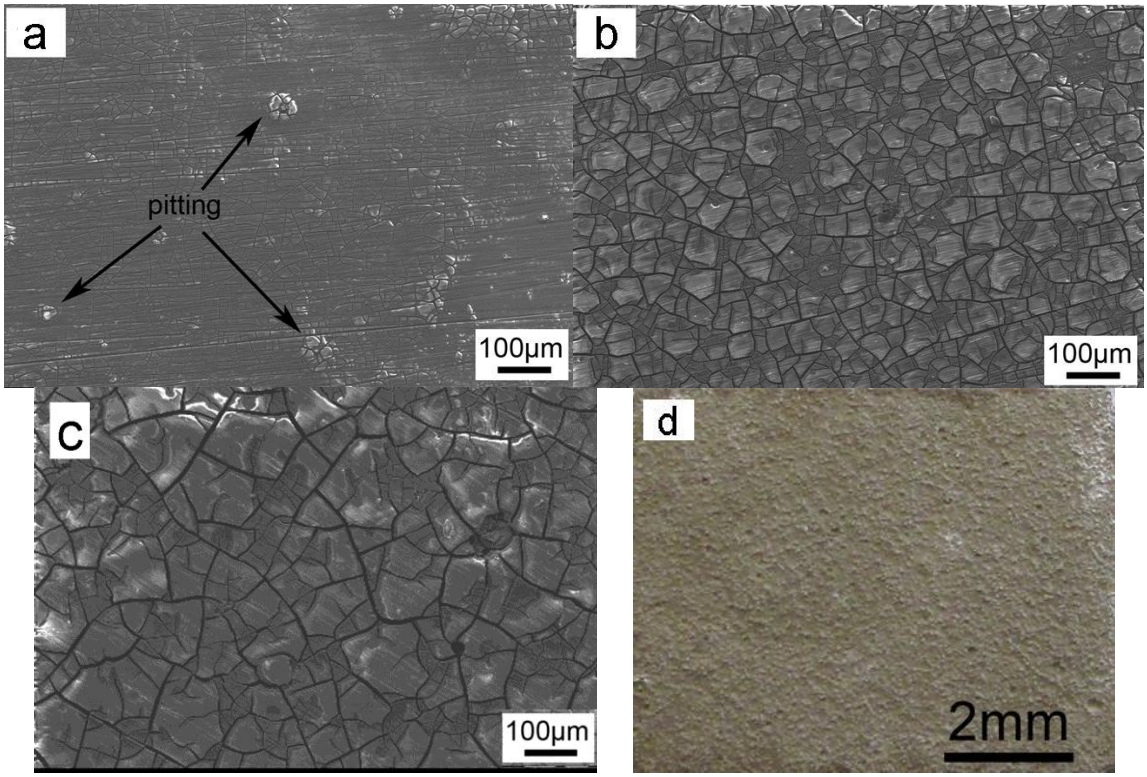

Fig. 15. Typical corrosion morphology of Mg-10Dy alloy after immersion for: (a) 1day; (b) 3 days; (c and d) 14 days. (a), (b) and (c) are SEM secondary electron images and (d) is an optical microscopy picture (after removing the corrosion products).

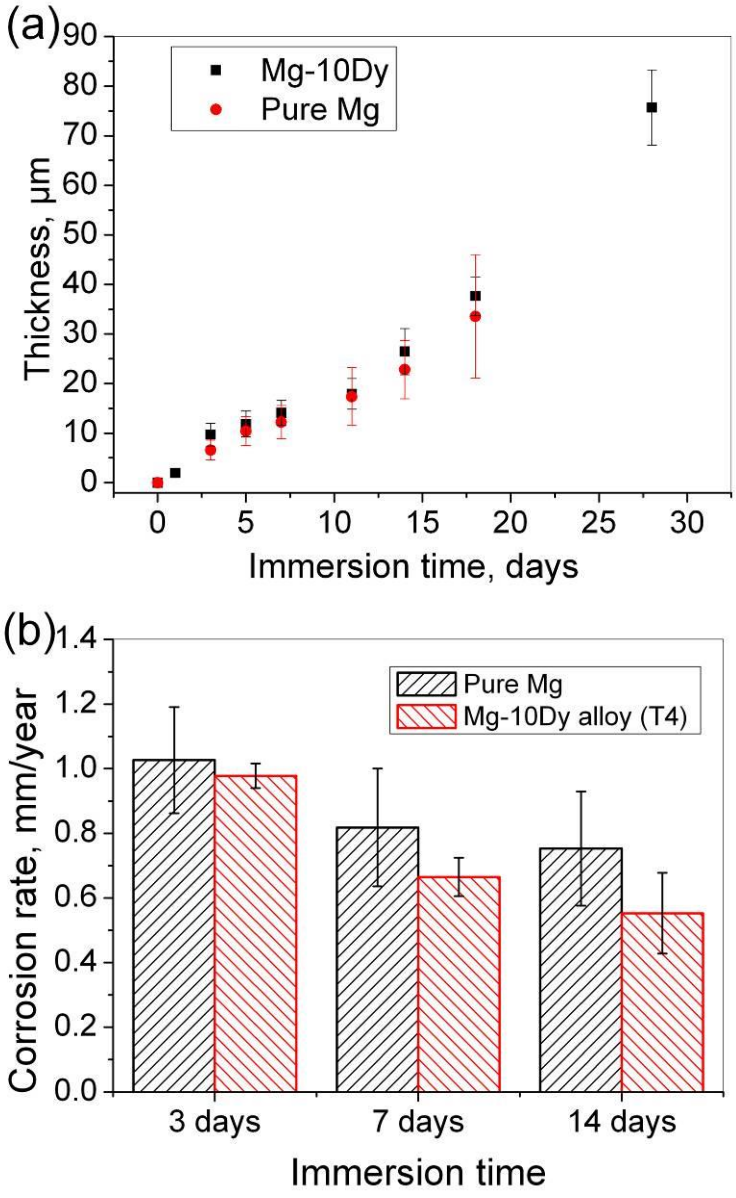

Fig. 16. (a) Thickness of corrosion layer and (b) Corrosion rate of pure Mg and Mg-10Dy alloy after immersion at different time points.

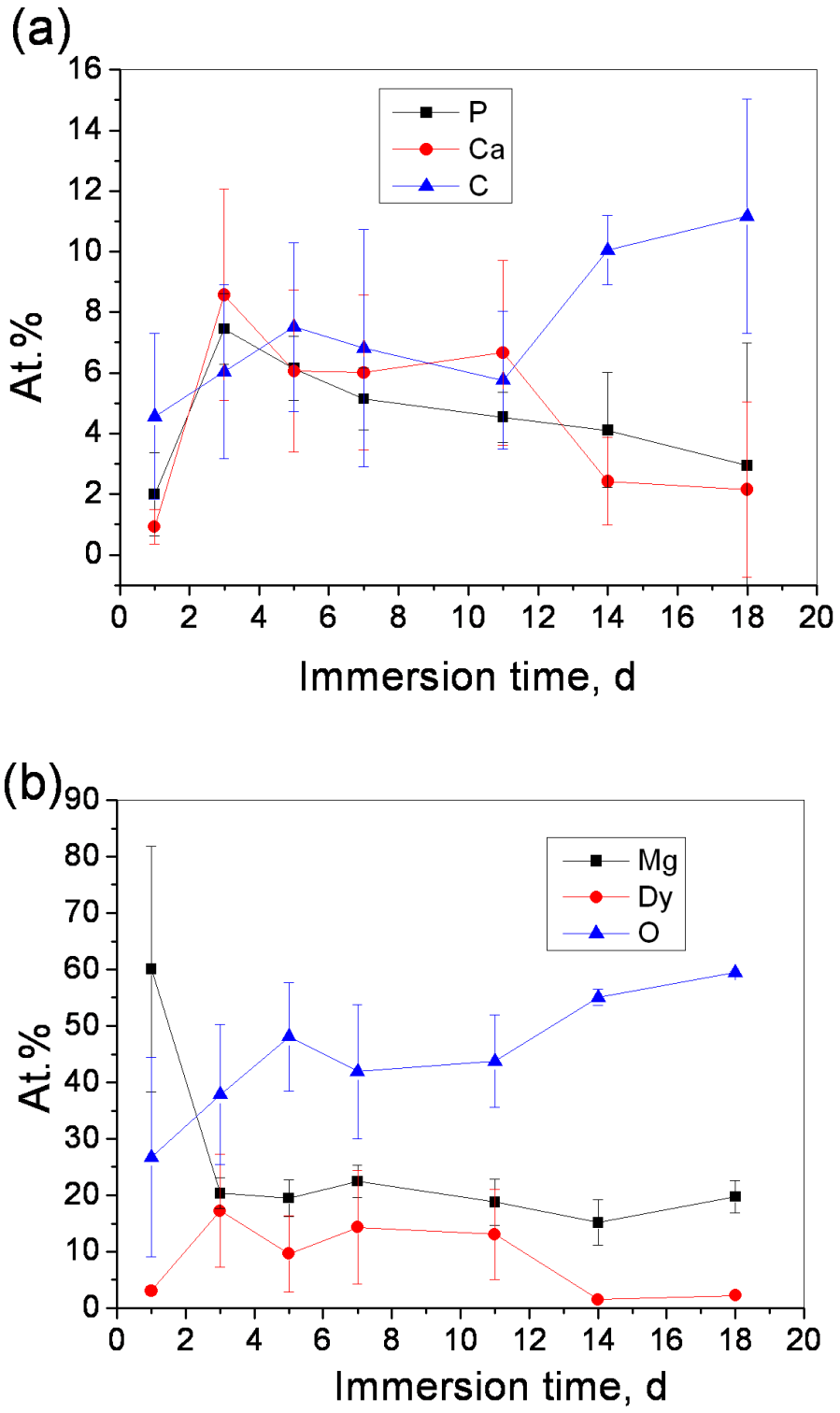

Fig. 17. Amount of main elements in the surface of the corrosion layer as a function of immersion time (analyzed by EDX).

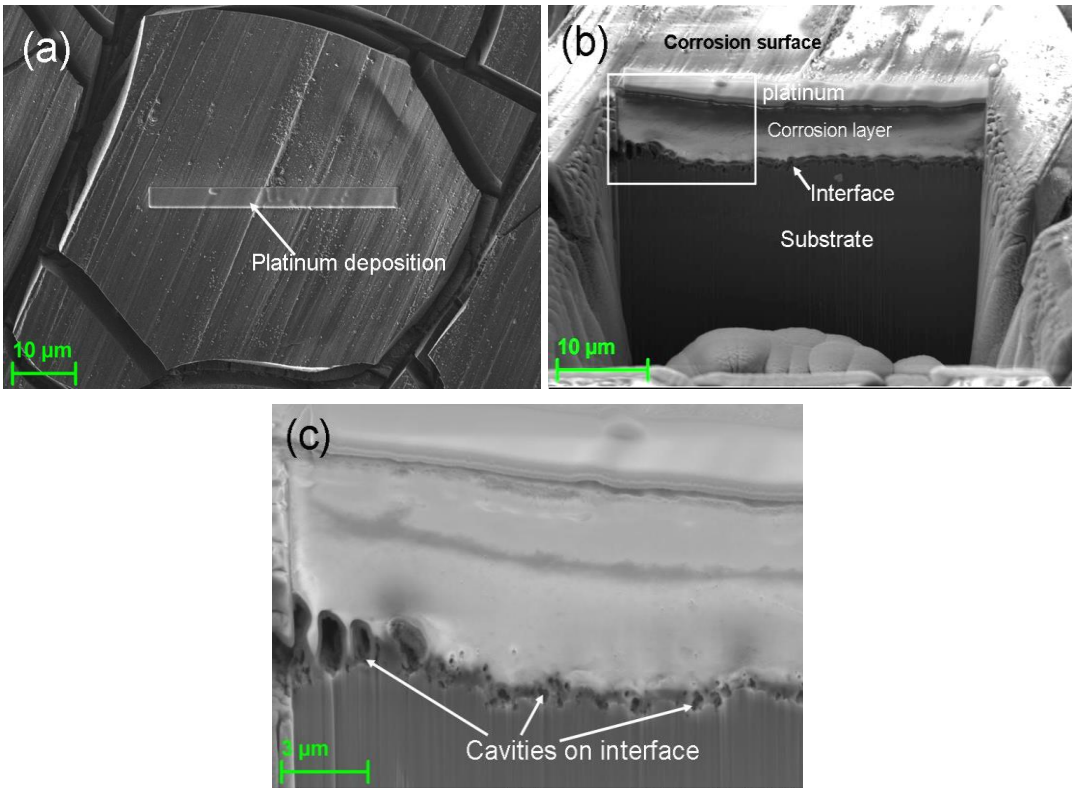

Fig. 18. SEM pictures showing the surface and cross-section morphologies of corrosion layer after immersion for 3 days: (a) cutting position on the surface; (b) cross-section at low magnification; (c) cross-section at high magnification.

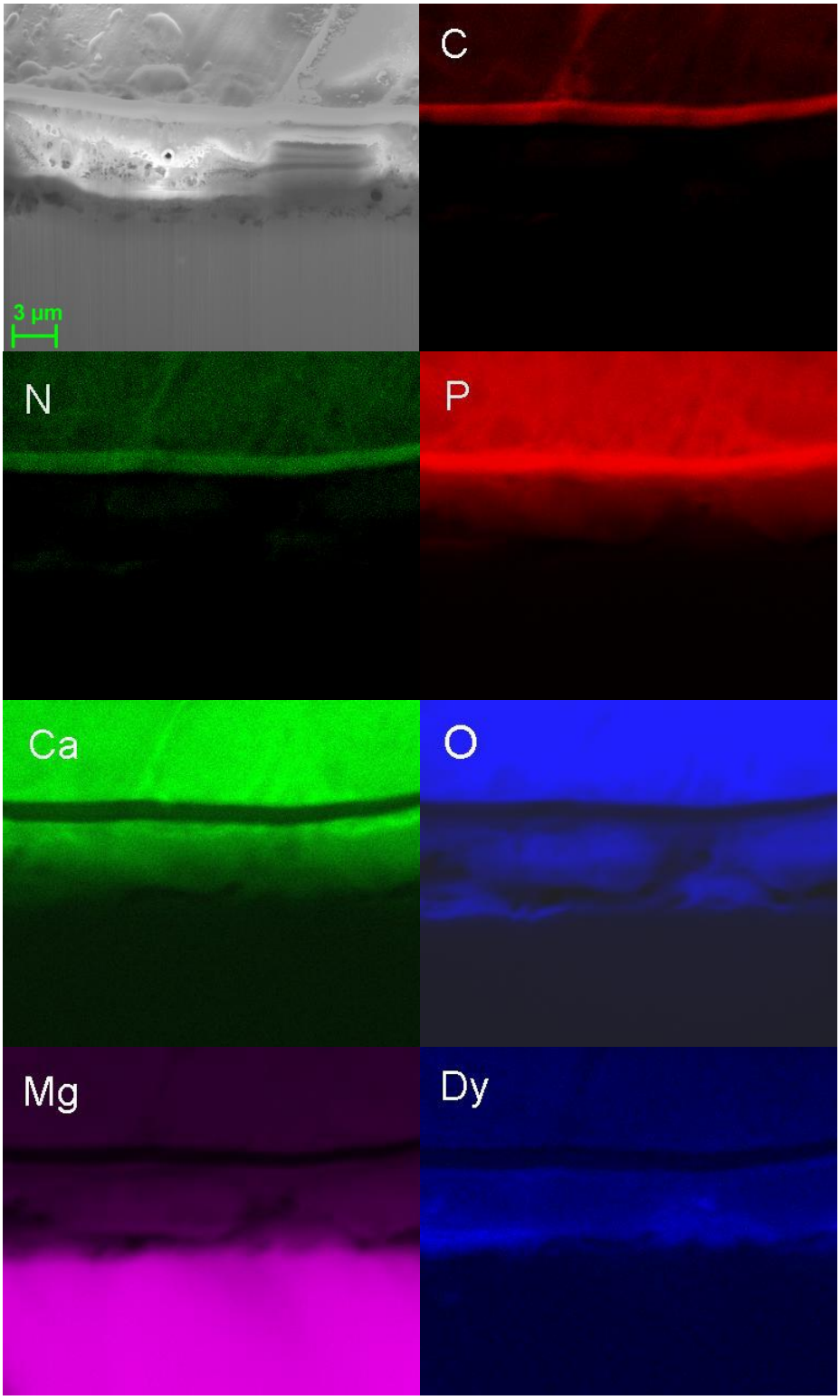

Fig. 19. Distribution of elements in the corrosion layer of the specimen after immersion for 3 days (EDX mapping).

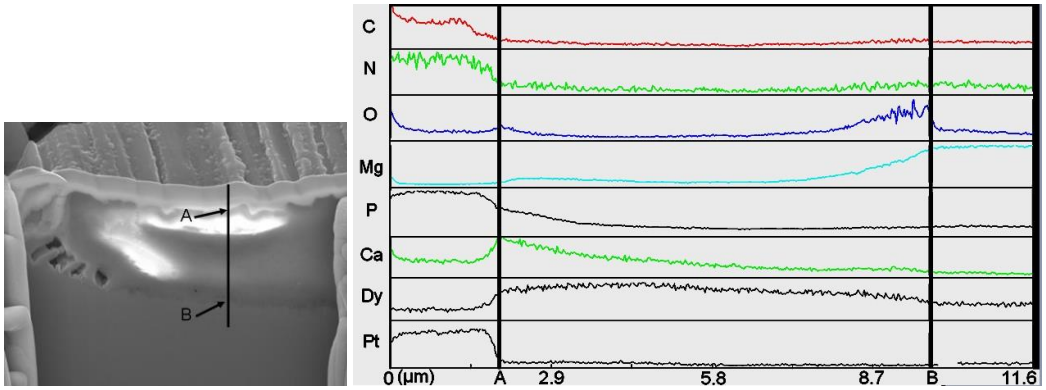

Fig. 20. Trend of element distribution in the corrosion layer (analyzed by EDX line scanning). The specimen was immersed for 3 days and cross section was cut with FIB. Bright area in the corrosion layer is due to a charge effect.

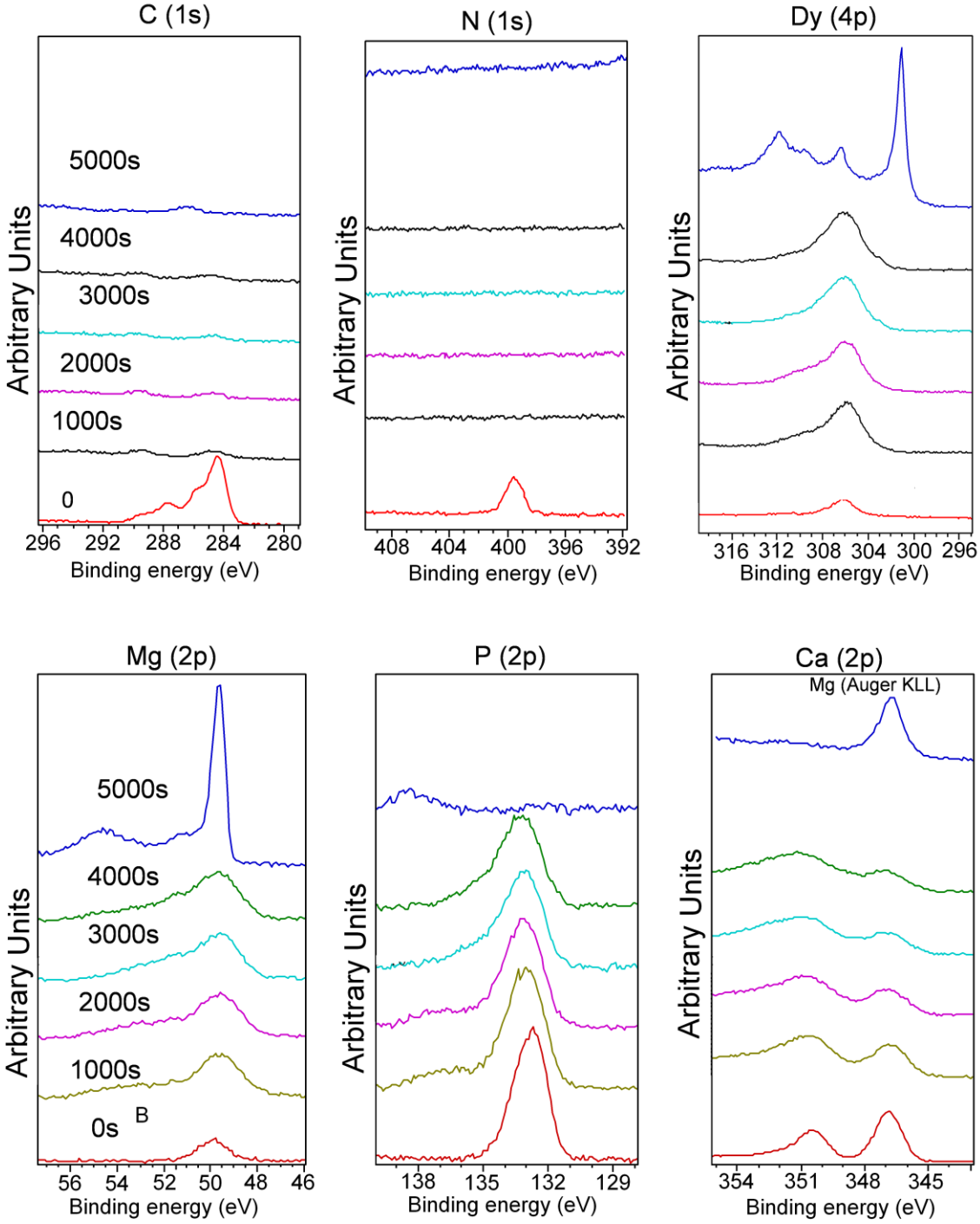
C (1s)
5000s
4000s
3000s
2000s
1000s
0
Arbitrary Units
296 292 288 284 280
Binding energy (eV)
N (1s)
Arbitrary Units
408 404 400 396 392
Binding energy (eV)
Dy (4p)
Arbitrary Units
316 312 308 304 300 296
Binding energy (eV)
Mg (2p)
5000s
4000s
3000s
2000s
1000s
0s
B
Arbitrary Units
56 54 52 50 48 46
Binding energy (eV)
P (2p)
Arbitrary Units
138 135 132 129
Binding energy (eV)
Ca (2p)
Mg (Auger KLL)
Arbitrary Units
354 351 348 345
Binding energy (eV)

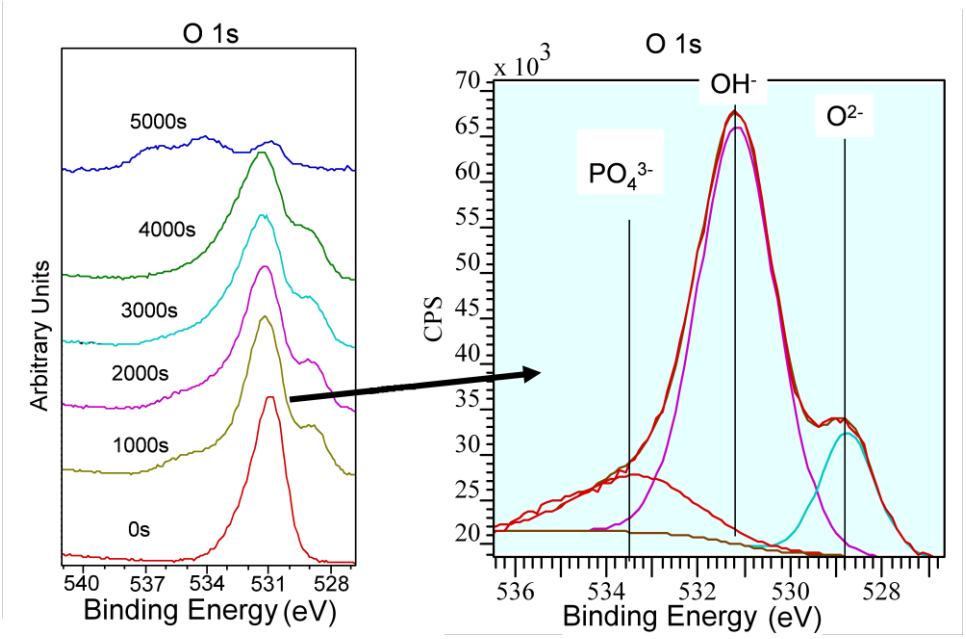

Fig. 21. XPS analysis of elements distribution in the corrosion layer of Mg-10Dy specimen after immersion for 1 day. 0-5000 s represents the etching time with argon ions before measurement.

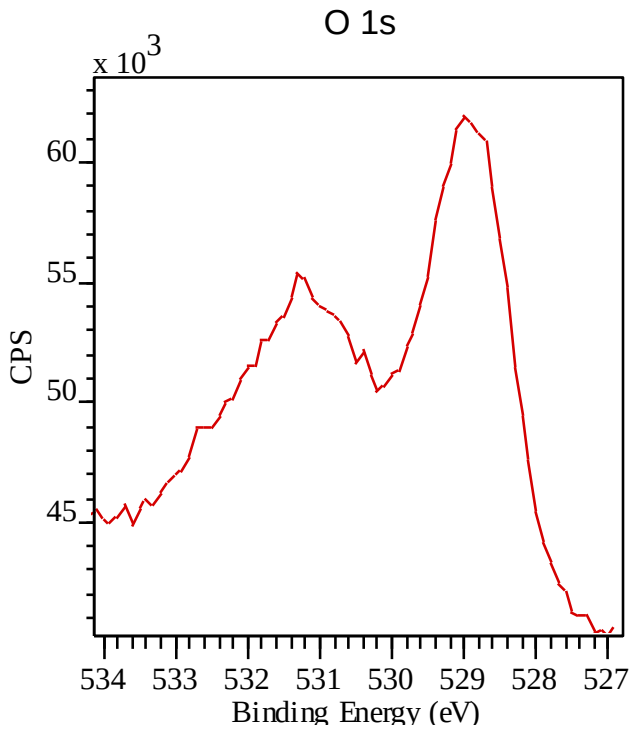

Fig. 22. XPS analysis of the corrosion layer on pure Dy metal after immersion in CCM for 1 day (after etching for 100 s).

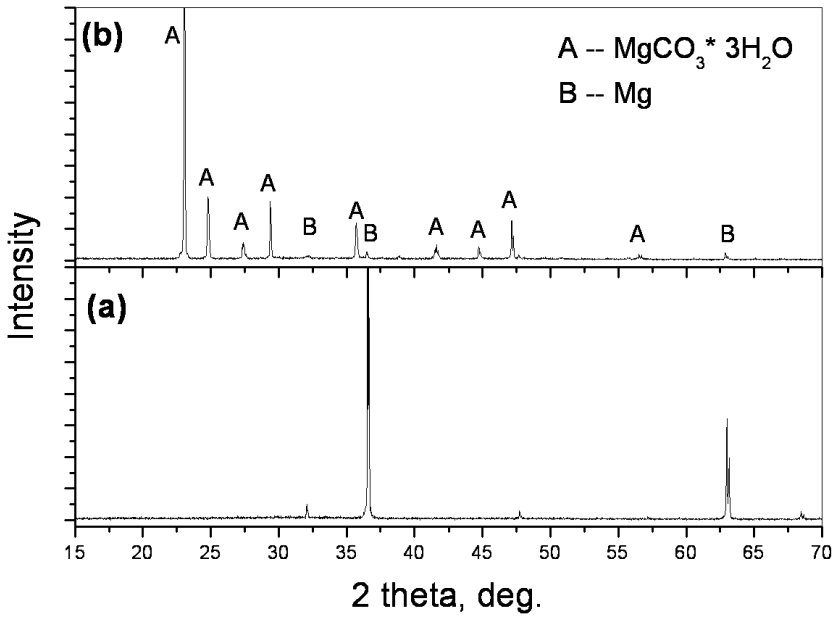

Fig. 23. XRD spectra of the corrosion layer on the surface of Mg-10Dy alloy after immersion for: (a) 14 days and (b) 28 days.

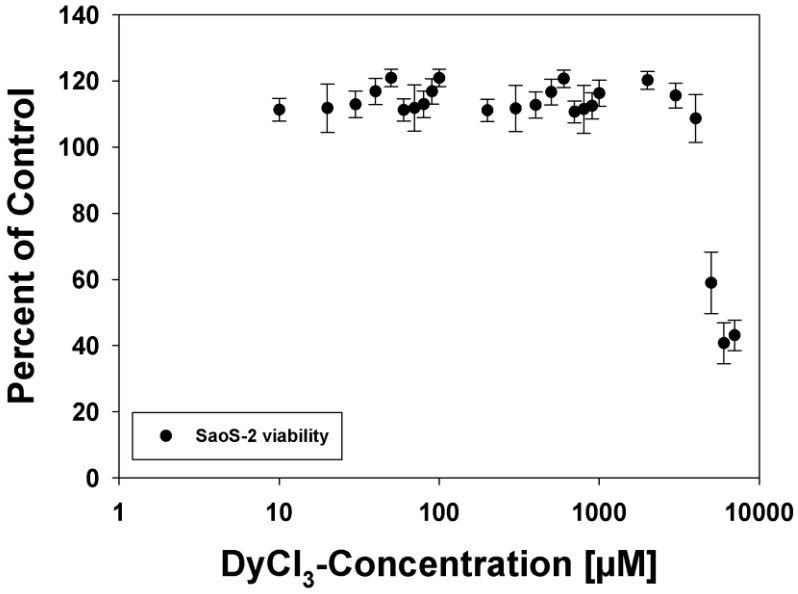

Fig. 24 Concentration-dependent dose response to exposure to DyCl3 of SaoS-2 cells.

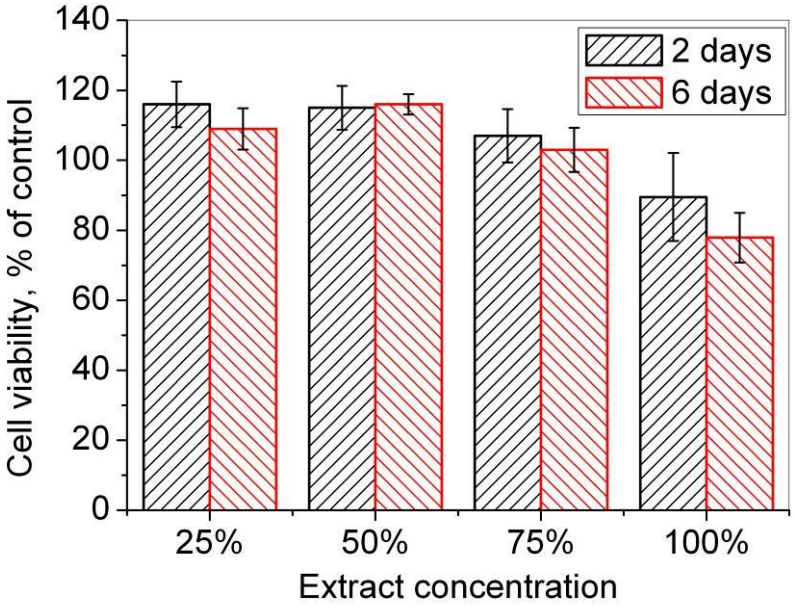

Fig. 25 Relative cell viability of osteoblasts after incubation in extracts for 2 and 6 days

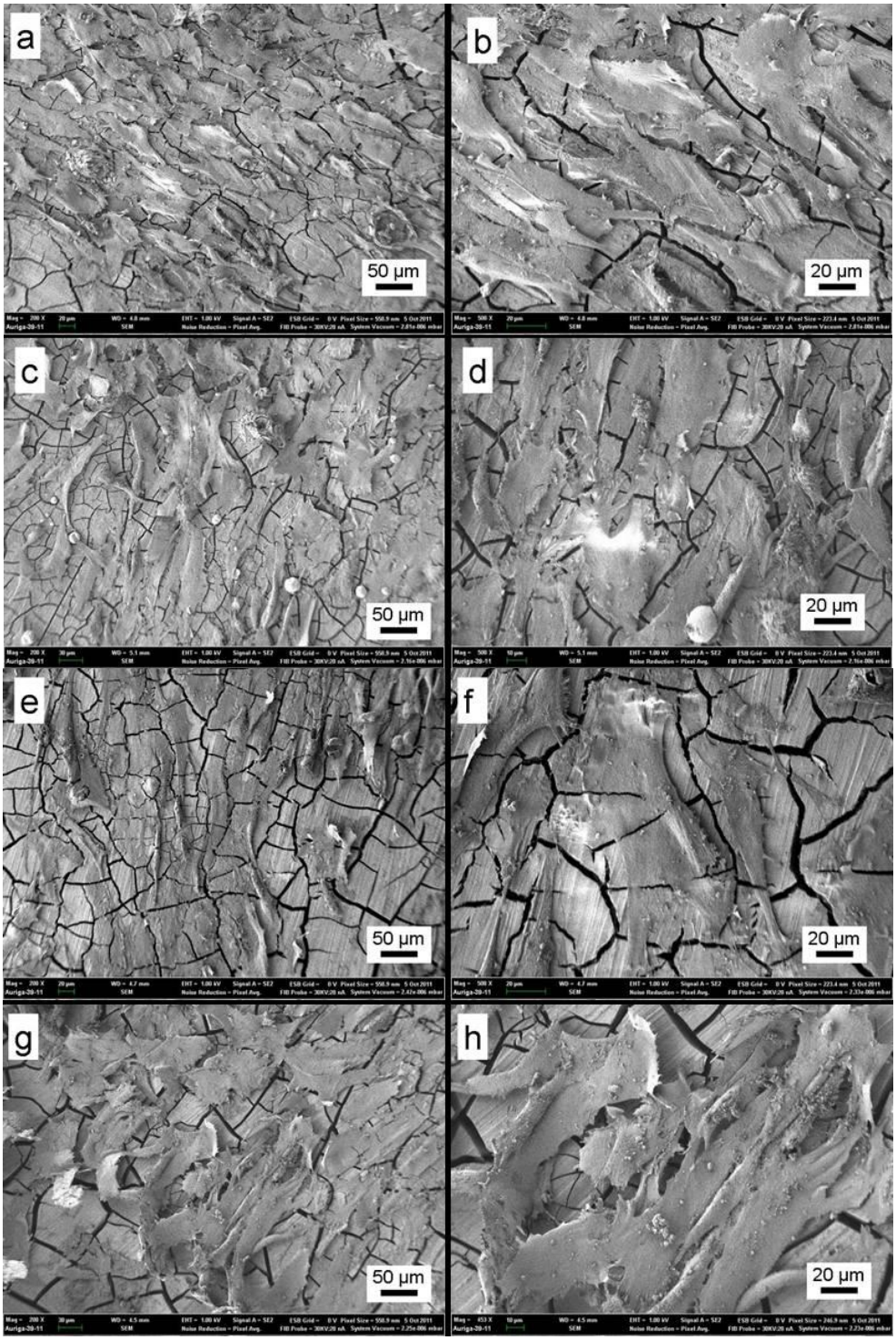

Fig. 26. Morphology of human osteoblasts on the surfaces of the specimens after culture for 3 days and 7 days: (a, b) pure Mg for 3 days; (c, d) Mg-10Dy for 3 days; (e, f) pure Mg for 7 days; (g, h) Mg-10Dy for 7 days. Prior to the cell seeding, the specimens were pre-incubated in CCM for 2 h.

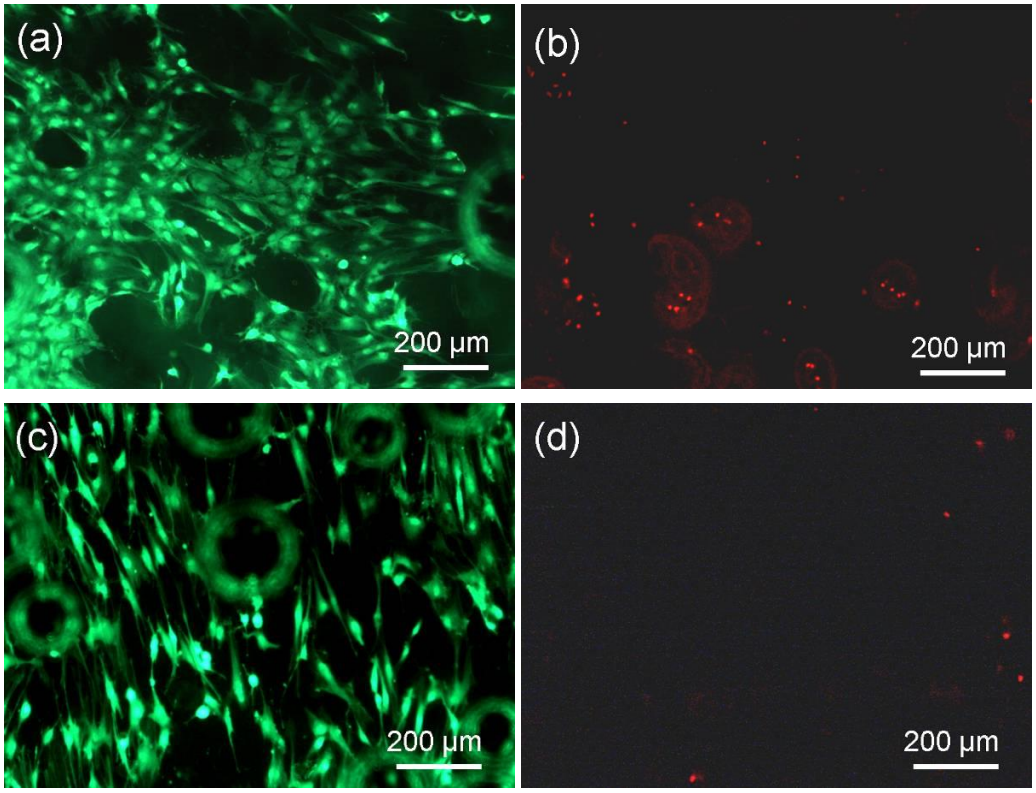

Fig. 27. Live (green) and dead (red) cells on the surfaces of specimens after culture for 3 days: (a, b) pure Mg; (c, d) Mg-10Dy alloy. Prior to the cell seeding, the specimens were pre-incubated in CCM for 3 days. The images of the live and dead cells were taken from the same locations. The round green circles shown in (a) and (c) are due to hydrogen bubbles.

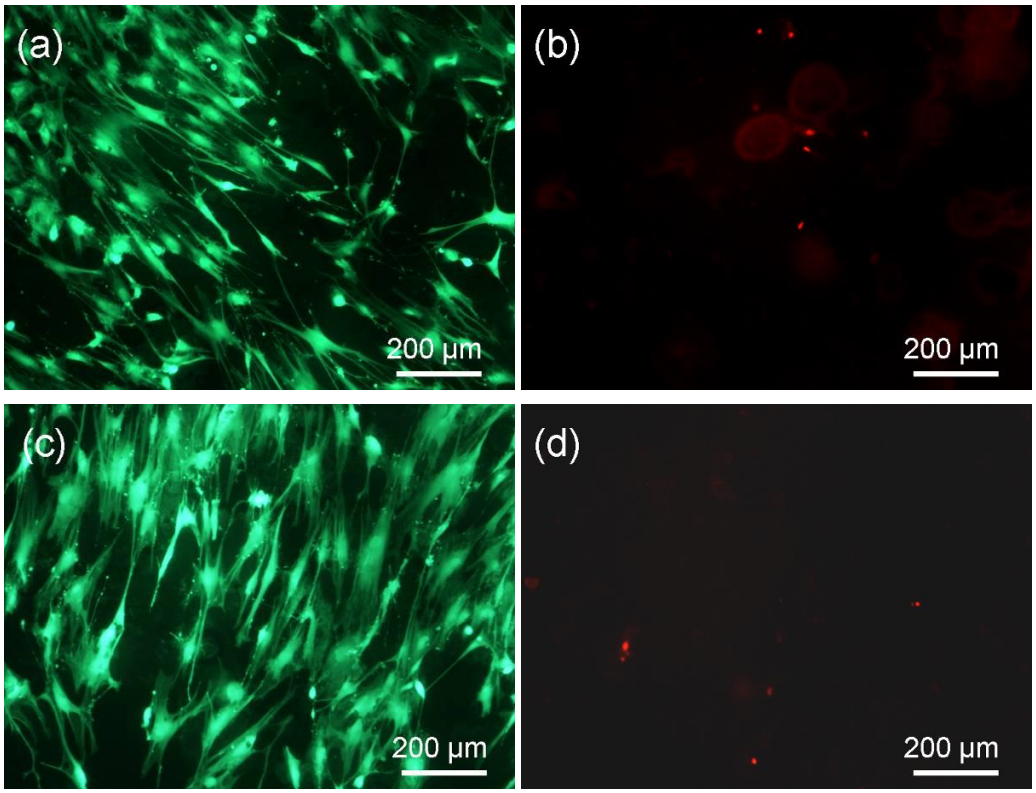

Fig. 28. Live (green) and dead (red) cells on the surfaces of specimens after culture for 7 days: (a, b) pure Mg; (c, d) Mg-10Dy alloy. Prior to the test, the specimens were pre-incubated in CCM for 3 days. The images of the live and dead cells were taken from the same locations.

Table 4 Detailed composition and impurity levels of Mg-10Dy alloy and pure Mg used in this work (wt.%).

	Dy	Fe	Ni	Cu	Mg
Mg-10Dy	9.2	0.005	<0.004	0.007	Balance
Pure Mg	---	0.005	<0.002	0.001	Balance

Table 5: Compositions of DMEM (mg/l).

Inorganic salts	Calcium Chloride ($CaCl_2 \cdot 2H_2O$)	264
	Ferric Nitrate ($Fe(NO_3)_3 \cdot 9H_2O$)	0.1
	Magnesium Sulfate ($MgSO_4 \cdot 7H_2O$)	200
	Potassium Chloride (KCl)	400
	Sodium Bicarbonate ($NaHCO_3$)	3700
	Sodium Chloride (NaCl)	6400
	Sodium Phosphate Monobasic($NaH_2PO_4 \cdot 2H_2O$)	141
Organic salts	Vitamins	35.6
	Amino Acids	1852
	D-Glucose (Dextrose)	4500
	Phenol Red	15
	Sodium Pyruvate	110

Table 6 Quantification of cell viability on the surfaces of pure Mg and Mg-10Dy alloy.

	3 days	7 days
Pure Mg	88.2±1.99	91.6±2.4
Mg-10Dy	94.3±2.5	92.5±2.7